PHYSICAL REVIEW D **91,** 083009 (2015)

Escape model for Galactic cosmic rays and an early extragalactic transition

G. Giacinti,[1] M. Kachelrieß,[2] and D. V. Semikoz[3]
[1]*University of Oxford, Clarendon Laboratory, Oxford, United Kingdom*
[2]*Institutt for fysikk, NTNU, Trondheim, Norway*
[3]*AstroParticle and Cosmology (APC), Paris, France*
(Received 10 February 2015; published 24 April 2015)

We show that the cosmic ray (CR) knee can be entirely explained by energy-dependent CR leakage from the Milky Way, with an excellent fit to all existing data. We test this hypothesis calculating the trajectories of individual CRs in the Galactic magnetic field. We find that the CR escape time $\tau_{\rm esc}(E)$ exhibits a knee-like structure around $E/Z = \text{few} \times 10^{15}$ eV for small coherence lengths and strengths of the turbulent magnetic field. The resulting intensities for different groups of nuclei are consistent with the ones determined by KASCADE and KASCADE-Grande, using simple power laws as injection spectra. The transition from Galactic to extragalactic CRs is terminated at $\approx 2 \times 10^{18}$ eV, while extragalactic CRs contribute significantly to the subdominant proton flux already for $\gtrsim 2 \times 10^{16}$ eV. The natural source of extragalactic CRs in the intermediate energy region up to the ankle are in this model normal and starburst galaxies. The escape model provides a good fit to $\ln(A)$ data; it predicts that the phase of the CR dipole varies strongly in the energy range between 1×10^{17} and 3×10^{18} eV, while our estimate for the dipole magnitude is consistent with observations.

DOI: 10.1103/PhysRevD.91.083009 PACS numbers: 98.70.Sa, 96.50.sb, 98.35.Eg

I. INTRODUCTION

The all-particle cosmic ray (CR) energy spectrum is a nearly featureless power law between $\sim 10^{10}$ and $\sim 10^{20}$ eV, with only a few breaks in its spectral index. The two most prominent ones are the knee at $E_{\rm k} \approx 4$ PeV, and the ankle at $E_{\rm a} \approx 4$ EeV. They must contain information about either CR sources or CR propagation. The range of possible theoretical explanations for these two breaks has been reduced in the last decade, but there is still no firm consensus on their origins. Another related open question is where the transition from Galactic to extragalactic CRs occurs. Unveiling this transition energy holds precious keys to understanding particle acceleration in the Universe. Other features have been observed in the spectrum between $E_{\rm k}$ and $E_{\rm a}$, see e.g. [1,2], and should contain additional clues.

In addition to the all-particle spectrum, both measurements of the primary composition and upper limits on the CR dipole anisotropy are crucial to constrain models of the knee and of the intermediate region up to the ankle. The KASCADE-Grande Collaboration has recently provided measurements of the intensities of individual groups of CR nuclei up to $E \approx 10^{17}$ eV [1,3,4]. Also, the IceTop Collaboration has presented measurements of the average of the logarithmic mass up to 30 PeV [5], while the Auger Collaboration deduced the contribution of individual CR groups to the total CR flux above $10^{17.8}$ eV from studies of the development of air showers [6,7]. In the region between the knee and the ankle, upper limits on the amplitude of the anisotropy have been reported, at roughly the percent level, by KASCADE [8], KASCADE-Grande [9], and Auger [10]. Below the knee, the dipole amplitude has been measured at the $\sim 10^{-3}$ level, by notably Super-Kamiokande (10 TeV) [11], MILAGRO (6 TeV) [12], EAS-TOP ($\approx$100 and 400 TeV) [13], IceCube (20 and 400 TeV) [14] and IceTop (2 PeV) [15].

For the knee, two main explanations currently remain possible. First, it may be the signature of the maximum energy to which Galactic CR sources can accelerate protons, see e.g. [16]. A nearby source could also leave such an imprint in the spectrum [17]. Second, the knee could be caused by a change in the energy dependence of the CR diffusion coefficient and thence confinement time in the Galaxy [18–20], if the CR Larmor radius is the order of the coherence length $l_{\rm c}$ of the turbulent Galactic magnetic field (GMF) at $E_{\rm k}$. In Ref. [20], we have studied this possibility—which we denote as the "escape model"—by propagating individual CRs in recent GMF models. This enabled us to avoid limitations from the diffusion approximation: While reliable analytical approximations for the diffusion tensor are only available in certain limiting cases, the diffusion approximation per se is not justified at the highest energies studied. We showed that the escape model is viable and can explain the individual fluxes of CR groups as measured by KASCADE and KASCADE-Grande. Moreover, our estimate for the dipole anisotropy in this model was consistent within uncertainties with observations.

In this work, we extend our previous study in Ref. [20] and formulate a model for the entire energy region between 300 GeV$/Z$ and the ankle. In addition to the Jansson-Farrar (JF) GMF model [21] used in [20], we consider the Pshirkov *et al.* (PTKN) model [22,23]. This enables us

to check the dependence of our results on the specific GMF model. Moreover, a more detailed study of the Galactic CR primary composition between E_k and E_a is presented here and compared to observations. We show that any remaining heavy nuclei flux in the sub-ankle region would be dominated by only one or few local sources. We use limits on the iron fraction at $\gtrsim 7 \times 10^{17}$ eV determined by the Auger Collaboration together with $\ln(A)$ measurements to constrain the transition energy between Galactic and extragalactic CRs, deducing $\mathcal{R}_{\rm max} = E_{\rm max,Fe}/(26e) \sim 10^{17}$ V as the maximal rigidity $\mathcal{R}_{\rm max}$ to which Galactic CR sources are able to accelerate CRs. The recovery of the proton and helium spectra above $E/Z \sim 10^{16}$ eV in the KASCADE-Grande data is mainly explained by the specific shape of the escape rate $\tau_{\rm esc}(E)$ discovered in [20]. We show also that observational constraints from anisotropy limits are compatible with the escape model. A natural extension of the escape model to other normal galaxies suggests that the extragalactic flux in the intermediate energy region up to the ankle is composed of CRs accelerated in starburst galaxies.

This article in organized as follows: In Sec. II, we test two GMF models for the regular and turbulent fields, as well as different strengths and coherence lengths for the turbulence. We deduce a range of models that fit constraints from notably the B/C ratio. We then compute in Sec. III the resulting fluxes of Galactic CR groups and show that they fit very well KASCADE and KASCADE-Grande measurements. In Sec. IV, we discuss the transition from Galactic to extragalactic CRs in our model. Finally, we review in Sec. V the constraints on and consequences of the escape model, before we present our conclusions in Sec. VI.

II. GALACTIC MAGNETIC FIELD MODELS, PARAMETERS FOR THE TURBULENCE AND CR CONFINEMENT IN THE GALAXY

A. Grammage

An important constraint on CR propagation models comes from ratios of stable primaries and secondaries produced by CR interactions on gas in the Galactic disk. In particular, the B/C ratio has been recently measured by the AMS-02 experiment up to 670 GeV/nucleon [24]. Above $E \gtrsim 10$ GeV/nucleon, these measurements for the B/C ratio are consistent with a straight power law.

In our previous work [20], we used a fit of the grammage performed in Ref. [25] using the leaky-box formalism and earlier data. In all cases considered in [25], the grammage traversed by CRs at reference energies $E_0/Z = (5\text{–}15)$ GeV was found to lie in the range $(9\text{–}14)$ g/cm^2. In order to take advantage of the high quality and the large energy range of the B/C data from AMS-02, we use now these data to derive the grammage traversed by CRs as function of their energies in two simple models. In the first one, we approximate the fraction of the B to C intensities by

$$\frac{I_B}{I_C} = \frac{p_{\rm sp}\lambda_s}{\lambda_B - \lambda_C}\left[\exp\left(\frac{X}{\lambda_C} - \frac{X}{\lambda_B}\right) - 1\right], \quad (1)$$

where $\lambda_i = m_p/\sigma_i$ are the interaction lengths (in gr/cm^2), σ_i the total inelastic cross section, m_p the proton mass and $p_{\rm sp} = \sigma_{\rm sp}/\sigma_{\rm tot}$ is the spallation probability deduced from the cross sections given in Ref. [26]. In the second approximation, we employ a fit function giving the B/C ratio directly as function of the grammage, following the approach in Refs. [27,28]. In Fig. 1, the grammage derived in Ref. [25] using earlier data is shown as black cross. The grammage deduced from the AMS-02 data using the first approximation is shown with magenta error bars, while the grammage obtained using the second approximation is shown with blue error bars. Note that the error bars take into account only the statistical and systematic errors of the AMS-02 measurement, while uncertainties in the cross sections or deficiencies of our approximations are not accounted for. The latter can be estimated by the differences between the results from the two approximations used.

In order to compare these measured values to those predicted in the escape model, we inject N cosmic rays at $z = 0$ in the Galaxy and follow their trajectories $\boldsymbol{x}_i(t)$ until they reach the edge of the Galaxy. As radial distribution of the injection points, we use

$$n(r) \propto (r/R_\odot)^{0.7} \exp\left[-3.5(r - R_\odot)/R_\odot\right] \quad (2)$$

with $[n] = \text{kpc}^{-2}$, assuming that the surface density of CR sources follows the distribution of supernova remnants in the Galaxy [29]. Here $R_\odot = 8.5$ kpc is the distance of the Sun to the Galactic center. We employ $n(z) = n_0 \exp(-(z/z_{1/2})^2)$ as model for the gas distribution in the Galactic disk, where z is the distance to the Galactic plane,

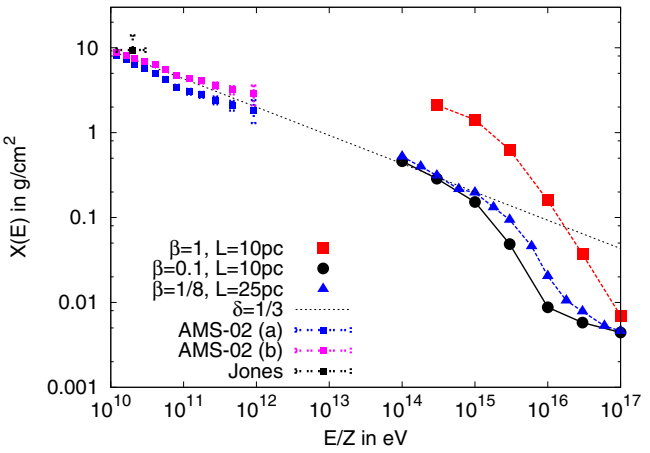

FIG. 1 (color online). Grammage for different coherence lengths l_c and turbulent fields: red squares $L_{\rm max} = 10$ pc and $\beta = 1$, black dots $L_{\rm max} = 10$ pc and $\beta = 0.1$, and blue triangles $L_{\rm max} = 25$ pc and $\beta = 0.125$, all cases for the JF GMF model [21]. Additionally we show the grammage deduced from B/C data.

$n_0 = 0.3/\mathrm{cm}^3$ at $R_\odot$ and $z_{1/2} = 0.21$ kpc inspired by [30]. We set $n = 10^{-4}/\mathrm{cm}^3$ as minimum gas density up to the edge of the Milky Way at $|z| = 10$ kpc. Then we calculate the average grammage $\langle X \rangle = N^{-1} c \sum_{i=1}^{N} \int dt \rho(\boldsymbol{x}_i(t))$ summing up the density along the trajectories of individual CRs. Since the grammage $X(E) \propto E^{-\delta}$ scales as the confinement time $\tau(E) \propto E^{-\delta}$, this quantity serves also as an indicator for changes in the CR intensity induced by a variation of the CR leakage rate.

B. Jansson-Farrar Model for the GMF

Let us recall first how the properties of a turbulent magnetic field determine the propagation of charged particles in the diffusion picture, before we discuss the specific case of the JF model. A turbulent magnetic field is characterized by its power spectrum $\mathcal{P}(\boldsymbol{k})$. The maximal length $L_{\max}$ of the fluctuations and the correlation length l_c are connected by $l_c = (\alpha - 1)L_{\max}/(2\alpha)$ for $\mathcal{P}(k) \propto k^{-\alpha}$. Assuming that the turbulent field is isotropic, the slope of the power spectrum $\mathcal{P}(k) \propto k^{-\alpha}$ determines the energy dependence of the diffusion coefficient $D(E)$ in the limit $E \ll E_{\mathrm{cr}}$ as $D(E) \propto E^{2-\alpha}$ on distances $l \gg L_{\max}$. Here, the critical energy E_{cr} is defined by $R_{\mathrm{L}}(E_{\mathrm{cr}}) = l_c$ and thus the condition $E \ll E_{\mathrm{cr}}$ ensures large-angle scattering, while the requirement $l \gg L_{\max}$ guarantees that features of anisotropic diffusion are washed out. Finally, we recall that the confinement time τ scales as the inverse of the diffusion coefficient.

In our previous work [20], we used the JF model for the regular and turbulent components of the Galactic magnetic field [21], choosing as the maximal length of the fluctuations $L_{\max} = 10$ pc. Note that for Kolmogorov turbulence the maximal length of the fluctuations $L_{\max}$ and the correlation length l_c are connected by $L_{\max} = 5l_c$ and that the diffusion coefficient scales as $D(E) \propto E^{1/3}$ for $E \ll E_{\mathrm{cr}}$. We considered two values of its root mean square (rms) strength, the original one suggested in [21] ($\beta = 1$) and a second one rescaling it to one tenth of its original value ($\beta = 1/10$).

In Fig. 1, we compare the grammage calculated from simulated CR trajectories for these two cases with the grammage deduced from B/C measurements. Because of the large energy reach of the AMS-02 data, the extrapolation required from the lowest energy of our numerical calculations, $E = 10^{14}$ eV, to the measurements has decreased to 2 orders of magnitude. Using the JF model with $\beta = 1$ as proposed in [21] would require a constant power spectrum of magnetic field fluctuations, $\mathcal{P}(k) \propto k^{-\alpha}$ with $\alpha = 0$, in the intermediate energy range. Such a power spectrum is difficult to reconcile with the theoretical understanding of turbulence. Moreover, the CR spectrum is very close to a power law above $\simeq$300 GV. This implies that if $D(E)$ would become significantly flatter beyond TeV energies [e.g. changing from $D(E) \propto E^{1/3}$ to $\propto E^0$], then the injection spectrum of sources has to have the exact opposite change of slope (e.g. respectively from $\propto E^{-2.4}$ to $\propto E^{-2.7}$). Alternatively, a change in the source density should compensate the change in $D(E)$ such that the observed CR intensity remains a nearly featureless power law [31]. Although such a conspiracy cannot be excluded, it appears to us as a not very attractive option.

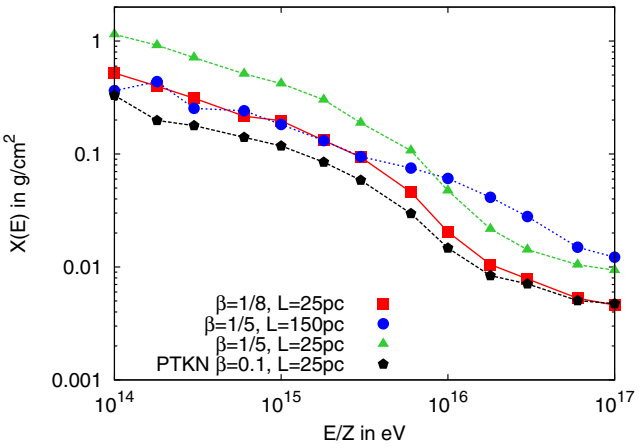

FIG. 2 (color online). Grammage for different coherence lengths l_c and turbulent fields: red squares $L_{\max} = 25$ pc and $\beta = 1/8$, blue dots $L_{\max} = 150$ pc and $\beta = 1/5$, and green triangles $L_{\max} = 25$ pc and $\beta = 1/5$, all cases for the JF model [21]. Additionally we show the grammage for the PTKN model with $L_{\max} = 25$ pc and $\beta = 0.1$ by black stars.

Choosing a Kolmogorov[1] power spectrum $\mathcal{P}(k) \propto k^{-5/3}$ as the theoretical model with the smallest slope α, we have to reduce B_{rms} therefore by a scaling factor $\beta < 1$ relative to the B_{rms} suggested in [21]. The exact value of β depends on the chosen coherence length l_c: A smaller coherence length leads to faster diffusion and thus to a smaller value of the grammage. For instance, a coherence length close to the upper limits derived in Ref. [32], $l_c = 5$ pc allows with $\beta = 1/8$ a somewhat weaker reduction in the level of the turbulence, cf. the blue line in Fig. 1. Increasing the coherence length even further to $l_c = 30$ pc, the scaling factor can be reduced to $\beta = 1/5$, cf. Fig. 2.

Next we examine how the shape of the grammage X as function of energy E/Z depends on the two parameters l_c and β. In [20], we discovered a specific shape of $X(E)$ that leads not only to a knee-like feature but reproduced also the recovery of the proton and helium spectra above $E/Z \sim 10^{16}$ eV, visible in the KASCADE-Grande data. From the examples in Figs. 1 and 2, it is clear that a too strong turbulent field, $\beta \sim 1$, results in knee-like feature at too high energy. Compensating a relatively strong turbulent field by decreasing the coherence length tapers off both the knee-like feature and the recovery, as shown by the case $l_c = 30$ pc in Fig. 2. As a consequence, the allowed range

[1]Note that a Kraichnan power spectrum ($\alpha = 3/2$) would require a stronger rescaling of the turbulent field, leading to a potential conflict with synchrotron data.

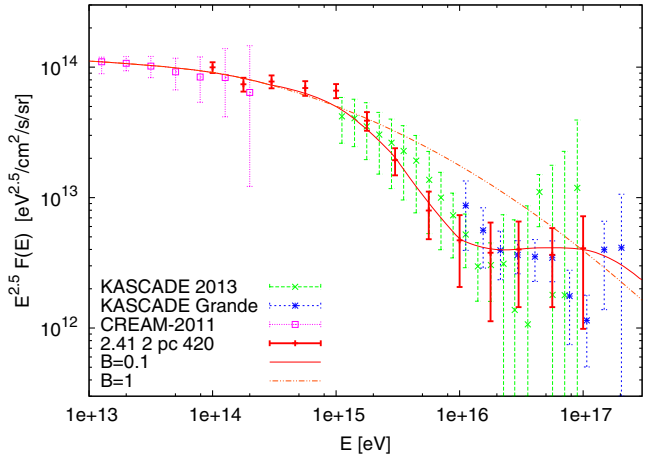

FIG. 3 (color online). Intensity using $I(E) \propto X(E)$ (red solid line) for the reduced turbulent field compared to the case of full turbulent field (red dashed line).

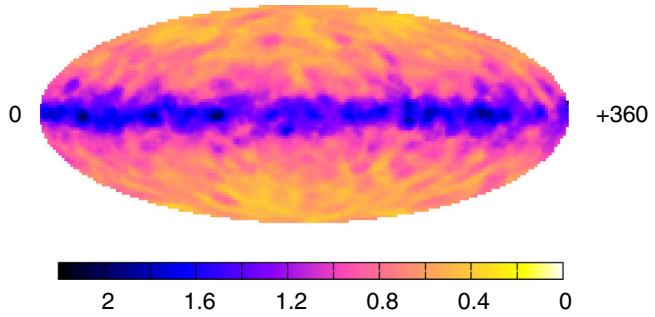

FIG. 4 (color online). Deflections of 40 EeV protons in a turbulent GMF realization with $L_{\max} = 100$ pc and $B_{\rm rms} = 5\ \mu{\rm G} \times \exp(-|z|/1.8\ {\rm kpc})$.

of turbulent field strengths and coherence lengths is correlated and very restricted, $l_c \simeq (1\text{–}10)$ pc and $\beta \simeq 1/10\text{–}1/8$.

This behavior is best illustrated comparing the modulation induced by the energy dependence of $X(E)$ on the intensity of protons to KASCADE and KASCADE-Grande data, and asking that a certain parameter choice reproduces the position and the shape of the proton knee. In Fig. 3, we show $I(E) = I_0(E)X(E)$, where in $I_0(E) = I_0(E/E_0)^\alpha$ the normalization I_0 and the slope α are chosen such to obtain a good agreement with observations below the knee for the case of full ($\beta = 1$, $L_{\max} = 10$ pc) and reduced ($\beta = 0.1$) turbulent fields with $L_{\max} = 10$ pc: This comparison demonstrates that only the case with reduced turbulence can reproduce the observed shape of the proton flux.

C. Pshirkov *et al.* Model for the GMF

In order to test the dependence of our results on the GMF model, we compute additionally the grammage $X(E)$ in the Pshirkov *et al.* model [22,23]. Its regular field consists of toroidal components in the Galactic halo, and of a disk field which follows spiral arms in the Galactic plane. We choose the bisymmetric benchmark model of [22], where the disk field presents reversals between consecutive arms. The authors of [22,23] did not present a three-dimensional model for the turbulent field. However, Pshirkov *et al.* [23] derived upper bounds on the deflections of ultrahigh energy CR (UHECR) induced by the turbulence magnetic field. Requiring that these bounds are satisfied allows us to construct a toy model of the turbulent GMF.

We choose $l_c = 5$ pc and as profile function $B_{\rm rms}(z) = B_0 \exp(-|z|/1.8\ {\rm kpc})$. Since the UHECR deflections at Earth as predicted by [23] do not show any significant dependence on the Galactic longitude, we neglect for simplicity a possible weak dependence of $B_{\rm rms}$ on the Galactocentric radius.

We backtrack individual 40 EeV protons from the Earth in a realization of isotropic Kolmogorov turbulence with such characteristics.[2] We compute their deflections on the sky, and present them in Fig. 4, after smoothing over 5° circles. One can see that 40 EeV proton deflections in such a turbulence are compatible with the fit for the upper limit on deflections from [23], both at high and low Galactic latitudes. For such a profile, the constraints at high latitude are more stringent than those close to the Galactic plane. Therefore, the results of Ref. [23] imply that, for a scale height of 1.8 kpc of the turbulent field, B_0 should not be significantly larger than $\approx 5\ \mu$G. We take this value in the following.

We can now compute the grammage in the PTKN model for the regular field, which we supplement by our toy model for the turbulent field. We find that we have to reduce the normalization B_0 of the turbulent field by a similar factor β as in the JF model: The case $\beta = 1/10$ and $l_c = 5$ pc is shown in Fig. 2 with black squares. Compared to our favorite cases in the JF model ($\{\beta = 1/8, l_c = 5\ {\rm pc}\}$ and $\{\beta = 1/10, l_c = 2\ {\rm pc}\}$), the qualitative behavior of $X(E)$ is very similar. It is therefore possible to limit the numbers of models, and we then decide to use the JF model for the rest of this study.

III. FLUXES OF GALACTIC CR GROUPS

A. Diffuse Fluxes from All Sources

In order to calculate the CR flux at Earth, we adopt the following procedure. First, we compute the three-dimensional CR density around a source at different times, and later use it as a template to infer the CR distributions around other sources. This allows us to reduce the required computing time and makes the problem tractable. For this template, we take a source located in the vicinity of the Earth and propagate individual CR protons from it in the GMF models which are presented in the previous section. We do this for CRs with energies between 100 TeV and

[2]In order to be compatible with the assumptions of [23], we have used $l_c = 50$ pc for this comparison.

100 PeV, and take four energies per decade. We divide the space around the source in cylindrical sectors with radii ranging from 0.1 to 4 kpc. We checked that the remaining contribution from the radial range 4–10 kpc does not change our results. Their widths in vertical direction depend on z and we choose their boundary lines as $|z| = 100$ pc, 200 pc, 300 pc, 400 pc, 500 pc, 700 pc, 1 kpc, 2 kpc, 3 kpc, 5 kpc, and 10 kpc. We divide time in bins of 5 kyr with a total of 6000 bins, up to $t = 30$ Myr. We checked also that the chosen bin sizes are small enough, in order to have no impact on the results. For every propagated CR, we save the fraction of its path in a given bin and average over all simulated particles. From this, we deduce the three-dimensional time-dependent CR density in the Galaxy for this source, and then for a distribution of sources.

We create the ensemble of CR sources as follows. We generate their positions within the Galactic disk ($|z| < 100$ pc), assuming that the density of CR sources follows the distribution given by Eq. (2). This distribution is assumed to depend only on the distance to the Galactic center, and not on the direction around it in the plane. The remaining parameters are the frequency of CR sources and the energy released in CRs by each of them. Only the product of these parameters is constrained by observations. We fix the energy released in CRs by each source to $E_{\rm tot} = 10^{50}$ erg, leaving the source frequency as the only free parameter. We sum up the contributions from these generated sources to the CR flux at Earth, in any time bin, and for a total duration of 300 Myr. For each energy bin, we save both the average flux at Earth and its one sigma deviation in time, i.e. the values of the flux where 16% of the cases are above and below the average. Note, that the upper and lower limits are not symmetric at high energies, since there are more cases with lower flux than average.

Results for nuclei with charge Z are deduced from the above calculations for protons by shifting the energy by a factor Z. We then interpolate the resulting CR nuclei fluxes to the same energies as for protons. At energies below $Z \times 100$ TeV, we assume that diffusion in the Kolmogorov turbulence shifts the injection power law $\propto E^{-\alpha}$ by $1/3$ to the spectrum $\propto E^{-\alpha-1/3}$ observed. This is indeed what we observe in our simulations in the energy range $\simeq Z \times (100\text{–}300)$ TeV. Therefore we assume that the CR spectrum of protons released by sources follows a power-law spectra $\propto E^{-2.4}$; the maximal energy E_p of protons will be fixed later by considering constraints from the resulting dipole anisotropy and the observed nuclear composition of CRs. For all other nuclei, we use power-law spectra with either $\propto E^{-2.17}$ or $\propto E^{-2.22}$ and maximal energy ZE_p. These power-law indices are chosen so as to fit the direct observations from CREAM at low energy. We fix the density of sources by normalizing the flux found in our simulations to the observed one at 100 TeV. On average, we require 440 sources per 100 kyr for a total energy per source of $E_{\rm tot} = 10^{50}$ erg, so as to fit the observed CR spectra. Within one time bin of 5 kyr we generate sources according to a Poisson distribution with an average of 22 sources, corresponding to the required source density on larger time scales.

In Fig. 5, we plot the CR nuclei fluxes, multiplied by $E^{2.5}$, as a function of energy. In the upper left and upper right panels of Fig. 5, we show the proton and helium fluxes, both for turbulent fields with $L_{\rm max} = 10$ pc and with $L_{\rm max} = 25$ pc. We plot orange lines $\propto E^{-2.4-1/3}$ (upper left panel) and $\propto E^{-2.22-1/3}$ (upper right panel), which represent the slopes expected theoretically at Earth, for our injection spectra with $\alpha = 2.4$ and 2.22 as power indices and Kolmogorov turbulence. Note that the slopes of the injection spectra required for nuclei, $\alpha \simeq 2.2$, coincide with the naive expectations from diffusive shock acceleration. Only the proton injection spectra requires a somewhat softer slope, $\alpha = 2.4$, than expected.

In the two upper panels, we show the experimental data from PAMELA [34] (orange points), CREAM [33] (magenta), KASCADE [4] (green) and KASCADE-Grande [4] (blue). The proton flux reported by KASCADE-Grande is 40% larger than the flux from KASCADE in the (10–30) PeV region, where the error bars of both experiments are relatively small. In contrast, the helium flux from KASCADE-Grande is below the one measured by KASCADE. This behavior may be explained by the insufficient discrimination power between protons and helium in the KASCADE-Grande experiment [35]. For this study, we choose therefore to reduce the proton flux of KASCADE-Grande by 40%, and add this difference to the helium flux, in same energy bins. By doing so, the CR fluxes of KASCADE-Grande and KASCADE experiments become consistent with each other.

In the lower left panel of Fig. 5, we plot the CNO flux, which predominantly consists of carbon and oxygen. We calculate the carbon and oxygen fluxes by normalizing them to the CREAM fluxes interpolated to higher energies with power laws, and then sum them up. The CREAM flux in this figure is the sum of its carbon and oxygen fluxes, where we use carbon energy bins for the binning, and interpolate the oxygen flux to these bins before summing up. KASCADE and KASCADE-Grande measurements of the CNO flux are directly compared to our fluxes.

In the lower right panel of Fig. 5, we show the flux of heavy nuclei, which is dominated by Mg, Si and Fe nuclei. Since the KASCADE and KASCADE-Grande Collaborations divide this flux in two parts ($\{\mathrm{Mg} + \mathrm{Si}\}$ and Fe), we also plot these two contributions separately in Fig. 6: Mg and Si in the left panel, and Fe in the right panel. It is possible to link the last points from CREAM to the first points from KASCADE-Grande with a smooth power-law, but not to those from KASCADE. This is likely to be due to the difficulty for KASCADE to distinguish between Si and Fe nuclei [35]. Therefore we choose to sum up the Mg, Si

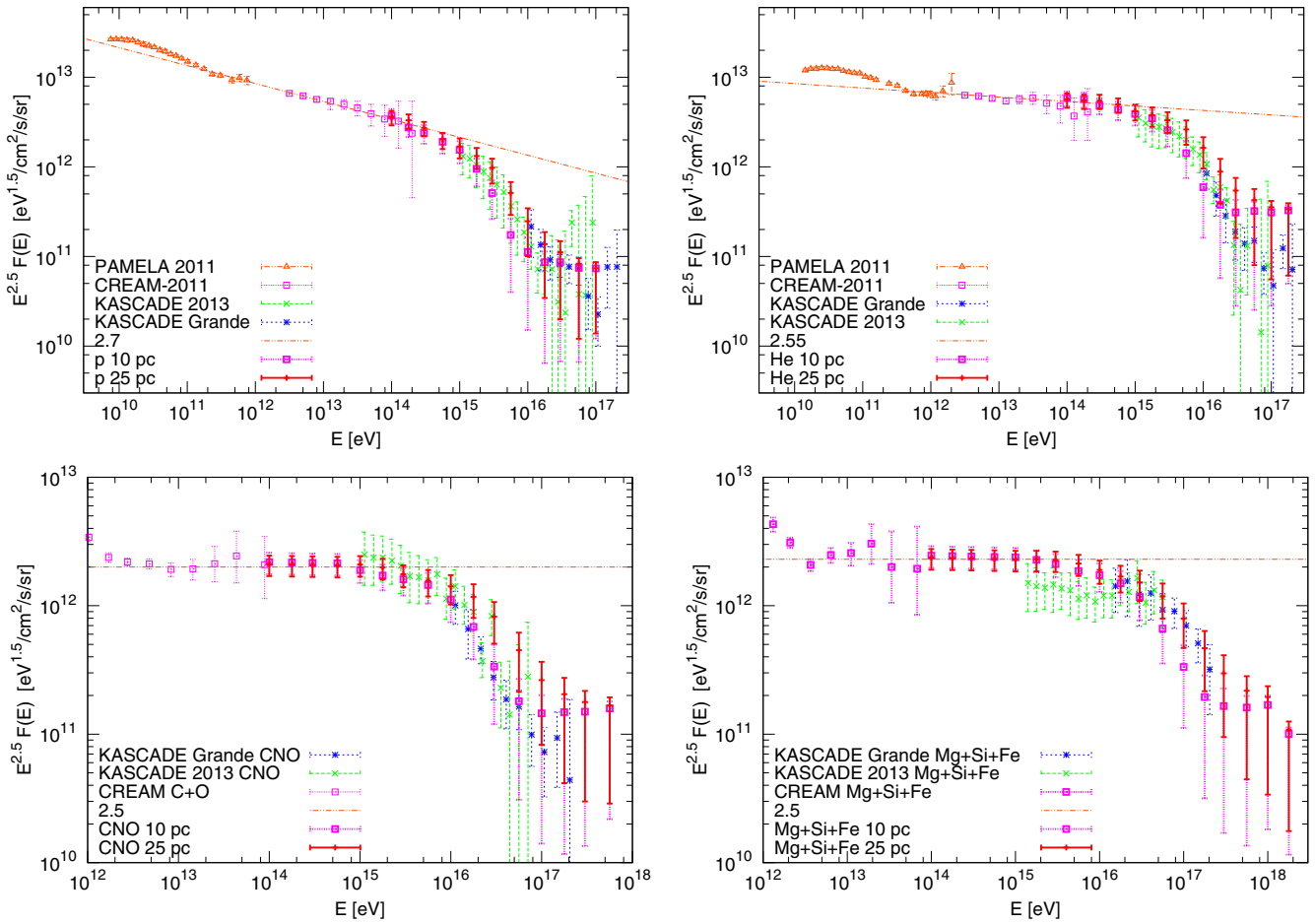

FIG. 5 (color online). Fluxes of CR protons (upper left), helium (upper right), carbon, nitrogen and oxygen (CNO) (lower left) and heavy elements including Mg, Si and Fe (lower right) are shown in red. Error bars show the variations in time of the fluxes. Experimental data from PAMELA for protons and helium, CREAM [33], KASCADE [4] and KASCADE-Grande [4].

and Fe fluxes into a single "heavy component" in the lower right panel of Fig. 5. In this figure, the combined "heavy nuclei flux" as measured by the KASCADE experiment is smooth and agrees well with a simple power-law extrapolation of the CREAM flux to higher energies. It also agrees with the KASCADE-Grande flux. As for the other components, the model presented in this work fits well the heavy nuclei flux too.

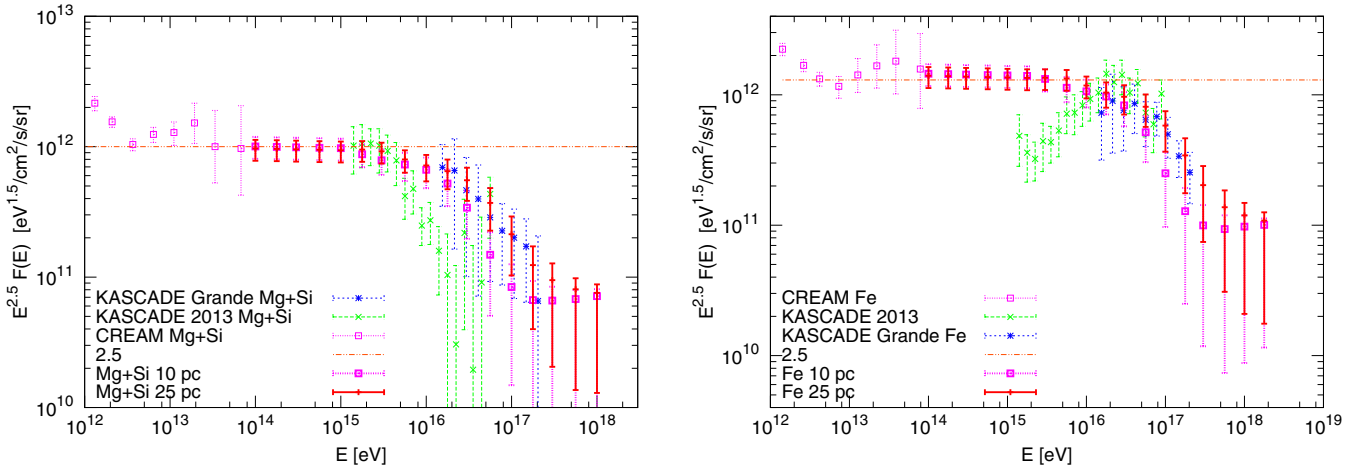

FIG. 6 (color online). Fluxes of Mg and Si (left) and Fe (right) are shown in red for $l_{\max} = 25$ pc and in blue for $l_{\max} = 10$ pc. Error bars show the variations in time. Experimental data from CREAM, KASCADE and KASCADE-Grande.

As can be seen in Fig. 5 (upper left), the CR proton flux follows a power law from 300 GeV up to about 1 PeV. It then changes to a steeper slope at the knee, and recovers at $\simeq$10 PeV to a flatter power law with index $\alpha \simeq 2.5$. Similar "knee-like" cutoffs, shifted by factors Z in energy, are visible in the fluxes of all groups of CR nuclei—see the other panels of Fig. 5. These plots demonstrate that the escape model fits very well all these observations. As discussed previously in [20], the knee is due, in this model, to a change in behavior with energy of the CR diffusion coefficient. The energy of the knee corresponds to the energy at which the Larmor radius of CR protons is of the order of the coherence length of the turbulent magnetic field ($l_c = L_{max}/5$ for a Kolmogorov spectrum). For the field strengths we consider in this paper, $B_{rms} \simeq 0.3\ \mu$G (or $\beta = 1/8$) averaged over a circle of radius 1 kpc distance from the solar position in the Galactic plane, we find in our calculations a change in the slope of the CR flux at about 1 PeV, as observed in the *proton* data.

B. Flux from Nearby Sources

In the escape model, the flatter part of the CR proton flux above $\simeq$10 PeV is dominated by recent nearby sources. This is due to the fact that the confinement time of CR protons in the Galaxy quickly drops with energy beyond the energy of the knee. The high-energy part, $E \gtrsim 3 \times 10^{17}$ eV, of the Galactic flux is dominated by heavy elements (Mg + Si + Fe). Recent nearby sources would dominate the flux of heavy elements at these energies. The composition study published by Auger in [7] constrains however the fraction of iron. Using conservatively the results obtained using the EPOS-LHC simulation, the iron fraction above 6×10^{17} eV is limited as $\lesssim$20%. We can add this constraint, excluding all time bins where the iron fraction exceeds this Auger limit. In the left panel of Fig. 7, we show experimental data for iron from CREAM, KASCADE and KASCADE-Grande together with the predicted iron flux without (blue error bars) and with accounting of the Auger iron constraint (red error bars). The maximally allowed iron flux using the composition constraint from [7] is shown as a magenta line. Since the signature of nearby, recent CR sources is a large iron fraction, the Auger constraint effectively eliminates these cases, resulting in a reduced flux at high energies, $E \gtrsim 10^{17}$ eV. In the right panel of Fig. 7, we show the same plot for protons.

Next we consider the effect of the Auger limit on the flux of the source which gives the maximal contribution at highest energy 100 PeV. The flux from this dominant source is shown in both panels of Fig. 7 without (blue circles) and with (red circles) accounting for Auger constraint on the iron fraction. In the former case, the dominant source contributes almost 100% of the proton flux at 5×10^{16} eV, while taking the Auger iron constraint into account reduces the dominance of the strongest source. Clearly, the relatively small fraction of iron observed by Auger disfavors the presence of a dominating source even at the end of Galactic CR spectrum.

Finally, we note that in the cases when the Auger iron constraint is violated, the total proton flux exceeds then the measured one and the knee-like structure is less pronounced than in the observed data. Above $Z \times 10^{16}$ eV, the predicted CR flux is dominated by a single nearby and recent source. Such a situation contradicts not only the Auger iron limit, but would violate also the limits on the dipole anisotropy of the CR flux: If one assumes that Galactic sources are able to accelerate only to energy just below the Auger constraint on iron, $E_{max} < 7 \times 10^{17}$ eV, the contribution of recent nearby sources is still limited by the Auger anisotropy limits, cf. the discussion in the next

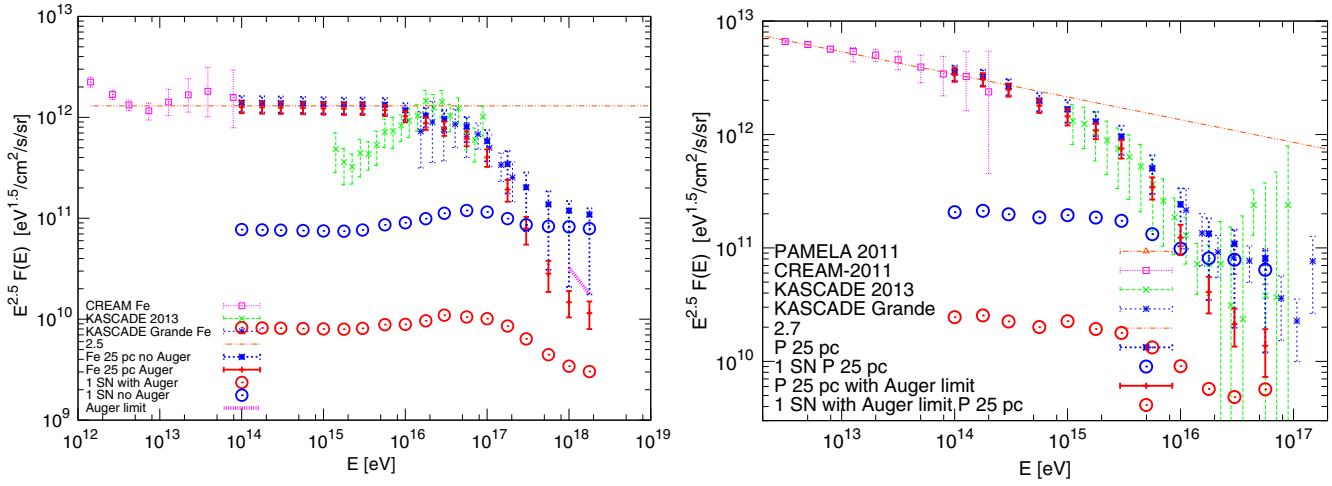

FIG. 7 (color online). Left panel: Experimental data for iron together with the predicted iron flux without (blue error bars) and with the Auger constraint (red error bars). Additionally, the iron flux from the dominant source is shown without (blue circles) and with Auger constraint (red circles). Right panel: The same plot for protons. All cases for $l_{max} = 25$ pc.

section. Thus the Auger limits on anisotropy and the iron fraction exclude the possibility that the highest energy part of the Galactic CR spectrum is dominated by a recent nearby source.

IV. TRANSITION FROM GALACTIC TO EXTRAGALACTIC CRS

Determining at which energy E_* the CR flux starts to be dominated by extragalactic sources is one of the most important unsolved problems in CR physics. While in the "dip model" of Ref. [36] the transition energy is as low as $E_* \approx$ a few $\times 10^{17}$ eV, the ankle has been in other models identified with the transition between Galactic and extragalactic CRs [37], $E_* \approx E_a \approx$ a few $\times 10^{18}$ eV. In our model, the energy of the transition E_* depends both on the maximum rigidity $\mathcal{R}_{\rm max}$ to which Galactic sources are able to accelerate CRs and on the distance to the nearest active source. As we have seen in the previous section, the Auger constraint on the iron fraction effectively eliminates the possibility that a single source dominates the high-energy part of the Galactic CR spectrum, reducing thereby the fluctuations.

We impose in the following the iron constraint throughout and assume that the end of the Galactic CR spectrum is determined by the maximum rigidity $\mathcal{R}_{\rm max}$ to which Galactic sources are able to accelerate CRs. Although $\mathcal{R}_{\rm max}$ is a free parameter in our model, the energy of the transition E_* can be determined by using additional observational constraints. One possibility is to constrain the maximum contribution of Galactic sources to the total CR flux by using the observational limits on the anisotropy of the CR flux. Another way to determine E_* is to study the elemental composition of primary CRs and to use the fact that the composition of Galactic and extragalactic CRs should in principle differ from one another.

We start with the latter method. As a first step, we derive the all-particle CR flux summing up all CR groups and compare it to the experimental data of KASCADE [38], KASCADE-Grande [1], TIBET [39], and Auger [40]. Then we deduce the extragalactic flux for a given $\mathcal{R}_{\rm max}$ by subtracting the predicted total Galactic flux from the measured total CR flux. The resulting extragalactic flux is shown in Fig. 8 with a red solid line for $\mathcal{R}_{\rm max} = 1.0 \times 10^{17}$ V. Next, we have to fix the nuclear composition of the extragalactic CR flux. As a first approximation, we can assume that its composition is constant in a sufficient small energy interval around E_*. In contrast, the Galactic CR composition is strongly energy dependent between the knee and the cutoff of the Galactic flux. Thus, we expect that an observable like the average of the logarithmic mass number, $\ln(A)$, will be quickly changing for $E \lesssim E_*$, while being approximately constant for energies slightly above E_*.

In Fig. 9, we plot measurements of $\ln(A)$ from several experiments, together with the values of $\ln(A)$ calculated within the escape model studied here. The points for

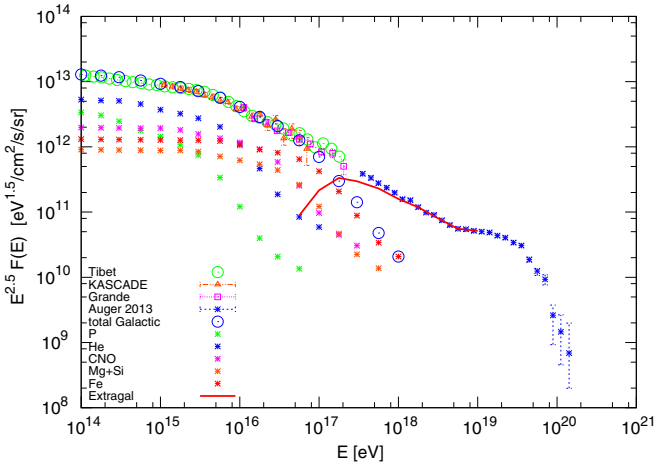

FIG. 8 (color online). CR flux and the extragalactic component we predict for $\mathcal{R}_{\rm max} = 1 \times 10^{17}$ eV, shown with the data from CREAM [33], KASCADE [38], KASCADE-Grande [1], TIBET [39], and Auger [40] experiments.

KASCADE have been computed by converting the flux measurements given in [4] into $\ln(A)$ values.[3] The most striking feature, namely the peak in $\ln(A)$ around 5×10^{16} eV, is clearly visible in all data sets, although its exact position and strength depend on the experiment. Our model reproduces the trend in the data very well. At higher energies, the composition becomes lighter because of the "flattening" of the escape time at such energies, see Sec. II. For the value of $\mathcal{R}_{\rm max}$ we consider here, extragalactic CRs start to contribute to the observed flux at $\approx 10^{17}$ eV. Consequently, above this energy, the exact value and shape of $\ln(A)$ depends on the assumed composition of the extragalactic flux. In blue, we show $\ln(A)$ for an extragalactic flux made of protons only, in magenta for a mix of 50% p and 50% Fe, and in red for a mix of 60% p, 25% He, and 15% N. Independently of the composition chosen for the extragalactic component, we can identify the energy where $\ln(A)$ stops to decrease with the maximum energy $E_{\rm max,Fe}$ to which Galactic sources can accelerate iron. It corresponds to the rigidity $\mathcal{R}_{\rm max} = E_{\rm max,Fe}/26e$. This transition is clearly visible in the PAO data, around the ankle, and allows us to determine the maximum rigidity as $\mathcal{R}_{\rm max} \simeq 1 \times 10^{17}$ V.

Accelerating Galactic CRs to $\mathcal{R}_{\rm max} \simeq 1 \times 10^{17}$ V is challenging, even for supernovas exploding in dense winds. However, several models in which one may reach such a high energy have been proposed. One possibility is the two-step acceleration of CRs in regions of OB star

[3]Recall that the KASCADE data for the heavy components showed a discrepancy to the extrapolation of the CREAM and KASCADE-Grande data and we had to sum them into a single heavy component. For the calculation of $\ln(A)$, we used instead the original fluxes for the separate CR groups what explains the small offset between our prediction and $\ln(A)$ deduced from KASCADE data at low energies.

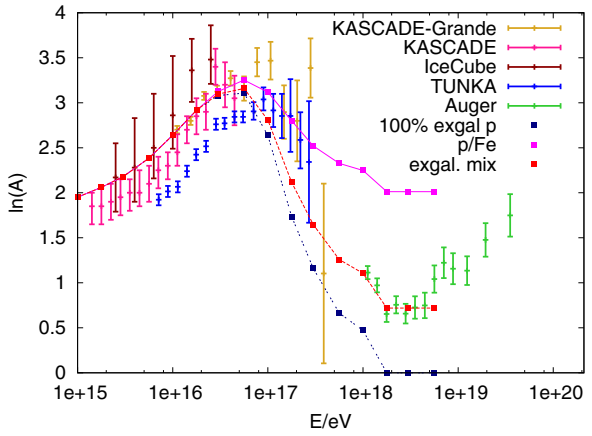

FIG. 9 (color online). Average of the logarithmic mass ln A predicted by our model for three different assumptions on the composition of extragalactic CRs, versus the experimental data.

formation, see Ref. [41] for a recent review. Since most of core-collapse SNe are located in superbubbles, CRs accelerated by individual SN remnants may be additionally accelerated in superbubbles to energies $\mathcal{R}_{\max} \simeq 1 \times 10^{17}$ V [41]. As another possibility, Ref. [42] suggests that CRs can be accelerated to ultrahigh energies at the termination shock of young pulsar winds. Note that in the early stages when the acceleration is most effective pulsars stay in the same OB regions, and the argument discussed applies in this case as well. The TeV gamma-ray emission from extended Galactic sources was studied in Ref. [43]. There it was found that the number of extended sources detected in Fermi data is consistent with the expected number of TeV CR sources. The majority of these TeV gamma-ray sources was associated with pulsars. If these gamma rays have a hadronic origin, pulsars may be candidates for the Galactic CR sources.

For the case of a mixture of 60% p, 25% He, and 15% N (red curve in Fig. 9), we obtain a good agreement with the $\ln(A)$ data from PAO up to 2×10^{18} eV. While this choice of composition is not unique, it is consistent with the results from the recent composition study published in [7]. In particular, Ref. [7] found the fraction of iron to be below 20% above 6×10^{17} eV. This agrees well with the results of our model, where the Galactic flux at 6×10^{17} eV consists purely of iron but contributes to only 15% of the total CR flux.

In addition to fitting the above observables, we still have to verify that the model presented here is also consistent with the existing upper limits on the CR anisotropy. In the diffusion approximation, the CR dipole anisotropy d is given by $\boldsymbol{d} = 3D\boldsymbol{\nabla}\ln(n)/c$. Following the same procedure as in [20], we compute the average anisotropy and derive the energy dependence of $D(E)$ from the escape rate as calculated previously, setting $D(E/Z) \propto 1/\tau_{\rm esc}(E/Z)$. We fix the proportionality constant by requiring that the dipole amplitude $d = \sum_k f_k d_k$ equals the dipole component $\tilde{d}$ observed by the EAS-TOP Collaboration at $E = 1.1 \times 10^{14}$ eV [13,44]. Here, k labels the groups of nuclei we consider in the Galactic flux plus an extragalactic component. The latter has a dipole amplitude which is independent of its composition and which we set equal to 0.6%, as expected for the extragalactic Compton-Getting effect [45]. The factor f_k corresponds to the fraction the component k contributes to the total CR flux, and $d_k \propto 1/\tau_{\rm esc}(E/Z)$ to their individual dipole. The relatively low value of the CR dipole measurements at TeV-PeV energies is known as the "CR anisotropy problem." Some authors have suggested that conditions of the local interstellar turbulence may be the cause [46,47].

In Fig. 10, we show the resulting dipole amplitude d as a function of energy E. As expected, the amplitude rises below the knee as $E^{1/3}$, while it increases approximately as $E^{0.7}$ until 1×10^{17} eV. At higher energies, the dipole amplitude decreases, which is due to the fact that the Galactic composition becomes heavier and that the extragalactic contribution grows. We also plot the values of $\tilde{d}$ observed by IceCube [14], as well as the 99% C.L. upper limits on $d_\perp$ from the Pierre Auger Observatory [10]. Comparing our estimate for the dipole amplitude with the upper limits in the energy range 10^{17}–10^{18} eV, we should take into account that the approximation $d \propto 1/\tau_{\rm esc}(E/Z)$ starts to break down above $E/Z \gtrsim 10^{17}$ eV, which leads to a sizeable error. We conclude therefore that our prediction is marginally consistent with these limits. The Pierre Auger Observatory should however be able to reach a detection of the dipole anisotropy. Let us also note that the escape model predicts that the phase of the dipole amplitude varies strongly in the energy range between 1×10^{17} and 3×10^{18} eV: This corresponds to the range where the transition from Galactic to extragalactic CRs lies. Such a picture is supported by current observations of the phase of the dipole, see Refs. [10,13,14].

In summary, there are two reasons for having an early transition, from predominantly Galactic to predominantly

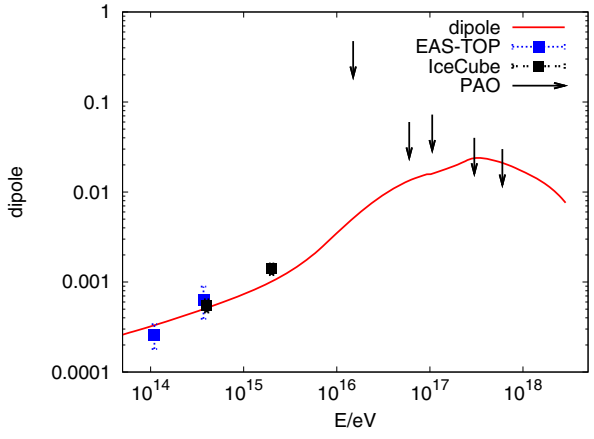

FIG. 10 (color online). Dipole amplitude $d(E)$ as a function of energy E in the GMF model of Ref. [21], using a reduced turbulent magnetic field with $\beta = 1/8$ and $L_{\max} = 25$ pc.

extragalactic CRs, at $E \approx$ a few $\times 10^{17}$ eV. First, the limits on the observed dipole anisotropy require either a very heavy Galactic composition or a predominantly extragalactic contribution at $E \gtrsim 10^{18}$ eV [10,48]. The former possibility is however strongly disfavored by the recent composition measurements from the Auger Collaboration [6,7]. Second, identifying the energy where $\ln(A)$ stops decreasing with the maximum energy to which Galactic sources can accelerate iron, $E_{\mathrm{max,Fe}} \approx 3 \times 10^{18}$ eV, suggests that the maximal rigidity reached in Galactic sources satisfies $\mathcal{R}_{\mathrm{max}} = E_{\mathrm{max,Fe}}/(26e) \sim 10^{17}$ V.

Finally, we comment on the contribution of extragalactic protons to the observed proton flux by KASCADE and KASCADE-Grande. In Fig. 11, we show these experimental data together with the predicted Galactic proton flux (red error bars), taking into account the Auger iron constraint. At $E \gtrsim 3 \times 10^{16}$ eV, the predicted Galactic proton flux lies below the measured one: Within the escape model, this difference should be accounted for by extragalactic protons. Subtracting the measured proton flux from the flux calculated in the escape model, we obtain a prediction for the extragalactic proton flux shown in magenta in Fig. 11. Note that the absolute value of this extragalactic proton flux is too small to impact the $\ln(A)$ plot, Fig. 9. We can check if the interpretation of this Galactic proton deficit in our model as an extragalactic flux makes sense comparing it to expectations at higher energies. We show therefore in Fig. 11 additionally the total CR flux (blue) measured by Auger. Applying the proton fraction from Ref. [7] obtained using the EPOS-LHC simulation we can then derive the resulting proton flux which is shown in magenta. To guide the eye, we plotted also a $E^{-2.2}$ power law with an exponential cutoff at $E = 2.4 \times 10^{18}$ eV as an orange line.

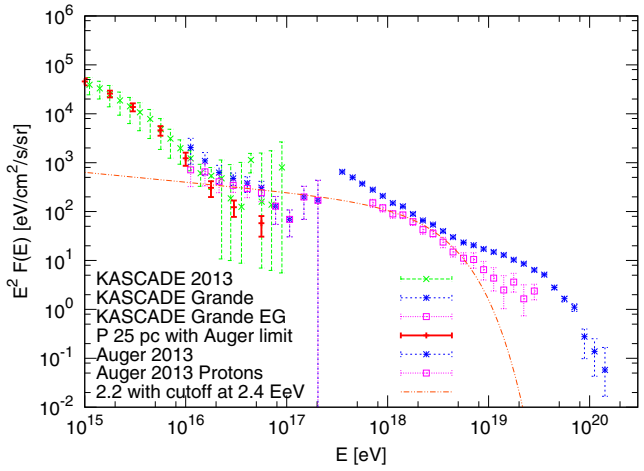

FIG. 11 (color online). The extragalactic proton flux deduced from the Auger and KASCADE-Grande data is shown in magenta together with the proton flux observed by KASCADE (green error bars) and KASCADE-Grande (blue error bars). The total CR flux from Auger (blue error bars) is shown together with the deduced proton flux (magenta error bars).

Such a $E^{-2.2}$ power law interpolates nicely between our prediction for the extragalactic proton flux using the KASCADE-Grande data and using the Auger data. This conclusion would not change using the spectrum and the composition measured by the Telescope Array, since the two experiments agree on the points that are the most important for our analysis: a very small fraction of iron and a large fraction of protons below 10^{19} eV. We conclude therefore that the extragalactic proton flux determined in the escape model, although with large errors, is consistent with the slope expected from shock acceleration and fits to the proton flux determined by Auger below the ankle.

V. DISCUSSION

Before we conclude, we review the main properties of the proposed escape model for Galactic CRs and the resulting consequences for the transition between Galactic and extragalactic CRs.

A. Constraints on the GMF

The escape model which aims at explaining the CR data from $E/Z \sim 300$ GeV to 100 PeV by the energy-dependent CR leakage from the Milky Way is strongly constrained by experimental data:

(1) The position of the knee, $E_{\mathrm{k}} \approx 4$ PeV, fixes a combination of the coherence length l_{c} and the strength of the magnetic field. Approximately, these parameters have to satisfy $l_{\mathrm{c}} \sim R_{\mathrm{L}}(E_{\mathrm{k}})$, while our numerical calculations show that the coherence length should lie in the range $l_{\mathrm{c}} = (2\text{–}5)$ pc for acceptable magnetic field strengths.

(2) The shape of the knee and, for large $\mathcal{R}_{\mathrm{max}}$, the subsequent recovery observed in the energy spectra of individual CR groups measured by KASCADE-Grande can be reproduced only if the turbulent magnetic field strength is smaller than assumed e.g. in the JF model of Ref. [21], cf. Fig. 3.

(3) A smaller strength of the turbulent field is also supported by B/C data: They constrain the grammage traversed by CRs and are consistent with a Kolmogorov-like power spectrum $\mathcal{P}(k) \propto k^{-5/3}$ of the turbulent field modes. Consistency with these measurements at lower energies also forces us to decrease B_{rms}. More quantitatively, we have to reduce the turbulent field in the JF model by a factor ~8, keeping the regular field unchanged.

(4) Such a reduction is in line with our determination of the diffusion coefficient in a purely turbulent magnetic field with strength $B_{\mathrm{rms}} = 4\ \mu$G [49], which also disagreed by an order of magnitude with the extrapolation of the diffusion coefficient phenomenologically determined from the ratio of secondary to primary nuclei.

Thus our model is based on relatively small values of the coherence length and the energy density in turbulent and regular magnetic fields. The first assumption is supported by a number of observational studies which derived limits on the coherence length in the Galactic disk of order 10 pc [32]. The second assumption appears more contrived, since the required reduction factor $\beta \approx 1/8$ is relatively large. However, we note that the recent study [50] suggests to rescale the isotropic turbulent field of the JF model by a factor 0.3, while it still predicts Faraday rotation measurements at low Galactic latitudes that are a factor 2 too large. Furthermore, a nonuniform density of electron in the Milky Way may lead to an overestimate of the turbulent Galactic magnetic field. Additionally, one should be aware that several oversimplifications in our analysis may lead to a somewhat too large value of β: For instance, we have not properly accounted for a possible anisotropy in the turbulent magnetic field or a spiral structure of CR sources in the Milky Way.

Let us note also that the weakness of the turbulent GMF in the escape model would have important consequence for the search of UHECR sources: UHECRs from a single source would be mainly deflected by the regular component of the GMF, while the spread of their arrival directions due to the turbulent GMF should be small. As a result, the search for UHECR sources, at least in the case of protons or light nuclei, should be easier than thought before. Even for heavier nuclei, the deflections in the regular field of the Galaxy can be traced back in those patches of the sky with small turbulent fields [51]. Weaker magnetic fields will also simplify the search of nuclei sources using the methods discussed in Refs. [52,53]. Thus the results of this work are an additional motivation for future searches of UHECR sources, performed by future all-sky missions as e.g. JEM-EUSO [54] and KLYPVE. [55].

B. Contribution of Starburst Galaxies

It is natural to apply the escape model to other normal galaxies. In particular, this model suggests that the CR knee in starburst galaxies is shifted by 2 orders of magnitude to higher energies [56], since the observed magnetic fields of these galaxies are a factor ∼100 larger than in the Milky Way [57]. Therefore, the extragalactic CR flux in the intermediate energy region up to ankle should be composed mainly of CRs accelerated in starburst galaxies. The ankle is then interpreted as the transition to another extragalactic source class, as e.g. active Galactic nuclei or gamma-ray bursts.

The flux of CRs escaping from starburst galaxies has a low-energy cutoff, when the interaction probability of CR nuclei on gas becomes of order one or the diffusion time in the intergalactic magnetic fields becomes comparable to the Hubble time. The magnetic horizon can be approximated at $E_{\rm cr} \lesssim E \lesssim 10^{18}$ eV by [58]

$$r_{\rm hor}^2 = \int_0^{t_0} {\rm d}t D(E(t)) = \int_{E_0}^{E} \frac{{\rm d}E'}{\beta} D(E') \approx \frac{c l_c}{H_0} \left(\frac{E}{E_{\rm cr}}\right)^2, \tag{3}$$

where H_0 is the Hubble constant and the critical energy $E_{\rm cr}$ is defined by $R_{\rm L}(E_{\rm cr}) = l_{\rm c}$.

Neither the strength nor the coherence length of the intergalactic magnetic field are well known. Lower limits on space-filling intergalactic magnetic field are around 10^{-17} [59], while the upper limit is given by $B \approx 0.1$ nG [60]. Using for illustration $B = 10^{-12}$ G and $l_{\rm c} = $ Mpc, the size of the magnetic horizon at $E = 10^{16}$ eV is for protons $r_{\rm hor} \sim 100$ Mpc and becomes comparable to the Hubble radius at $E = 3 \times 10^{16}$ eV. Since the magnetic horizon of nuclei is smaller, a further prediction of this scenario is that the extragalactic flux is initially purely composed of protons, becoming at higher energies heavier and more similar to the Galactic composition. This is in line with our finding of an extragalactic *proton* contribution above 3×10^{16} eV, cf. Fig. 11, and a proton dominated extragalactic flux deduced from the $\ln(A)$ data.

The low-energy cutoff due to interactions of CR nuclei on gas can be estimated by rescaling Fig. 1. For magnetic fields a factor 100 larger, significant attenuation of the CR nuclei sets in below 10^{16} eV. Thus we assume that the CR flux reaching the Milky Way from starburst galaxies is not affected strongly by interactions or magnetic confinement in the for us interesting range $E \gtrsim 3 \times 10^{16}$ eV. Detailed calculations of the diffuse CR flux from starburst galaxies will be presented in Ref. [61].

C. Connection to Diffuse Neutrino and γ-Ray Fluxes

The recent discovery [62,63] of astrophysical neutrinos with energies $E > 10$ TeV by the IceCube experiment opened a new field—high-energy neutrino astrophysics. The measured astrophysical neutrinos events are not completely uniformly distributed over the sky, but have an overdensity towards the Galactic plane and a region close to the Galactic center. In Ref. [64], it was suggested that these neutrinos are secondaries from CR interactions in the central part of our Galaxy. Later it was shown that the observed neutrino spectrum, which follows the power law $1/E^{2.45}$ [63], has the same slope and normalization as the all-sky gamma-ray spectrum measured by the Fermi-LAT experiment [65] at lower energies [66]. It was suggested that both spectra are dominated by hadronic interactions of CRs in our Galaxy. In this case, the CR spectrum in the central part of the Milky Way should be consistent with a $1/E^{2.5}$ power law, which in turn agrees with the slope of the nuclei spectrum derived in this work. Taking into account the change of the power-law exponent by $1/3$ in the case of Kolmogorov turbulence, such a spectrum is consistent with the slope $1/E^{2.2}$ suggested by acceleration models.

An exception is the locally measured proton spectrum, which has the spectrum $1/E^{2.7}$. As argued in Ref. [66], such

a spectrum could by caused "recent" (i.e. within ∼10 Myr) variation of the local CR flux due to a nearby source. Such an event might be connected to the creation of the Gould belt of molecular clouds. The aged proton spectrum of such source would be softer than the average spectrum of Galactic "sea" CRs, while CR nuclei have been spallated except of at very low rigidities. Finally, we note that the main contribution to the observed amplitude of the dipole anisotropy at $E \lesssim 10^{14}$ eV could be caused by this source, exceeding thereby the $1/E^{1/3}$ low-energy continuation of our estimate presented in Fig. 10 [67].

The flux of astrophysical neutrinos contains a significant fraction of neutrinos outside the Galactic plane, which should have an extragalactic origin. In the framework of the present model, these extragalactic neutrinos should be created by CR interaction in normal and starburst galaxies. As discussed in Ref. [66], they can explain both a significant part of the diffuse gamma-ray background and of the IceCube signal outside the Galactic plane [61].

D. Source Rate and the Slope of the Injection Spectra

In our model, we use as average injection spectrum of CRs a constant power law $dN/dE \sim E^{-\alpha_i}$ for each group of CR nuclei over the rigidity range 200 to 10^8 GV. This suggests that a single source class accelerates the CRs observed in this energy range. These sources should either all accelerate to $\mathcal{R}_{\rm max} \simeq 1 \times 10^{17}$ V, or their maximal rigidities should follow approximately a power-law distribution [31]. Since the required maximal energy in our model is high, one expects that only a subset of all Galactic CR accelerator is responsible for the CRs in this energy range. This is in line with our determination of the source rate, 0.4/century, that is a factor 10 lower than the usually assumed SN rate.

Because of the large leverage in our fits, the resulting constraints on the exponents α_i are much tighter than considering only, e.g., CREAM data: Rather steep power laws with, e.g. $\alpha_p \simeq 2.65$ for the observed proton spectrum, which cannot be excluded by CREAM data alone are incompatible adding KASCADE and KASCADE-Grande data.

VI. CONCLUSIONS

We have shown that the knee can be entirely explained by energy-dependent CR leakage from the Milky Way, with an excellent fit to *all* existing data from $E/Z \sim 300$ GeV to 100 PeV. In particular, all deviations from a single power-law behavior that are observed in the CR intensity of individual CR groups in the energy range $E/Z \sim 200$ GeV up to 100 PeV are consistently explained by rigidity-dependent CR escape. This model requires small coherence lengths of the turbulent field and relatively small turbulent magnetic fields. If these two conditions are fulfilled, then the CR escape time $\tau_{\rm esc}(E)$ exhibits a knee-like structure around $E/Z = \text{few} \times 10^{15}$ eV together with a recovery around $E/Z \simeq 10^{16}$ eV.

We have determined the maximal rigidity $\mathcal{R}_{\rm max} = E_{\rm max,Fe}/(26e) \sim 10^{17}$ V to which Galactic CR sources are able to accelerate CRs by identifying it with the energy where $\ln(A)$ derived from PAO measurements stops to decrease. The resulting flux ratio of Galactic and extragalactic sources is in our model 1:1 at $E_* \approx 2 \times 10^{17}$ eV, dropping to 0:1 at 2×10^{18} eV. The extragalactic CR flux in the intermediate energy region up to ankle should be composed mainly of CRs accelerated in starburst galaxies. Since the transition from Galactic to extragalactic CRs happens in this model at rather low energies, the estimated CR dipole anisotropy is consistent within uncertainties with upper limits in the energy range 10^{17}–10^{18} eV, while it reproduces the measurements at lower energies from EAS-TOP and IceCube. The dipole phase is expected to change between 1×10^{17} and 3×10^{18} eV, i.e. the energy range of the transition from Galactic to extragalactic CRs. Such a behavior corresponds to the one observed, providing thus additional evidence for a transition from Galactic to extragalactic CRs in this energy region.

ACKNOWLEDGMENTS

We would like to thank Andreas Haungs for discussions about the KASCADE and KASCADE-Grande data and Michael Unger for sending us data files of the $\ln(A)$ values derived in [68]. M. K. thanks the Theory Group at APC for hospitality. G. G. acknowledges funding from the European Research Council under the European Community's Seventh Framework Programme (FP7/2007–2013)/ERC Grant Agreement No. 247039. The work of D. S. was supported in part by Grant RFBR No. 13-02-12175-ofi-m.

[1] W. D. Apel *et al.* (KASCADE-Grande Collaboration), The spectrum of high-energy cosmic rays measured with KASCADE-Grande, Astropart. Phys. **36**, 183 (2012).
[2] M. G. Aartsen *et al.* (IceCube Collaboration), Measurement of the cosmic ray energy spectrum with IceTop-73, Phys. Rev. D **88**, 042004 (2013).
[3] W. D. Apel *et al.* (KASCADE-Grande Collaboration), Kneelike Structure in the Spectrum of the Heavy Component of Cosmic Rays Observed with KASCADE-Grande, Phys. Rev. Lett. **107**, 171104 (2011).
[4] W. D. Apel *et al.* (KASCADE-Grande Collaboration), KASCADE-Grande measurements of energy spectra for

elemental groups of cosmic rays, Astropart. Phys. **47**, 54 (2013).
[5] R. Abbasi *et al.* (IceCube Collaboration), Cosmic ray composition and energy spectrum from 1–30 PeV using the 40-string configuration of IceTop and IceCube, Astropart. Phys. **42**, 15 (2013).
[6] A. Aab *et al.* (Pierre Auger Collaboration), Depth of maximum of air-shower profiles at the Pierre Auger Observatory: Measurements at energies above $10^{17.8}$ eV, Phys. Rev. D **90**, 122005 (2014).
[7] A. Aab *et al.* (Pierre Auger Collaboration), Depth of maximum of air-shower profiles at the Pierre Auger Observatory: Composition implications, Phys. Rev. D **90**, 122006 (2014).
[8] T. Antoni *et al.* (KASCADE Collaboration), Large scale cosmic-ray anisotropy with KASCADE, Astrophys. J. **604**, 687 (2004).
[9] C. Curcio *et al.* (KASCADE-Grande Collaboration), Proceedings, 33rd International Cosmic Ray Conference (ICRC2013), Braz. J. Phys. **44**, 415 (2014).
[10] P. Abreu *et al.* (Pierre Auger Collaboration), Constraints on the origin of cosmic rays above 10^{18} eV from large scale anisotropy searches in data of the Pierre Auger Observatory, Astrophys. J. **762**, L13 (2012); Large scale distribution of arrival directions of cosmic rays detected above 10^{18} **eV** at the Pierre Auger Observatory, Astrophys. J. Suppl. Ser. **203**, 34 (2012); I. Sidelnik *et al.* (Pierre Auger Collaboration) (to be published).
[11] G. Guillian *et al.* (Super-Kamiokande Collaboration), Observation of the anisotropy of 10 TeV primary cosmic ray nuclei flux with the Super-Kamiokande-I detector, Phys. Rev. D **75**, 062003 (2007).
[12] A. A. Abdo *et al.*, The large scale cosmic-ray anisotropy as observed with Milagro, Astrophys. J. **698**, 2121 (2009).
[13] M. Aglietta *et al.* (EAS-TOP Collaboration), Evolution of the cosmic ray anisotropy above 10^{14} eV, Astrophys. J. **692**, L130 (2009).
[14] R. Abbasi *et al.* (IceCube Collaboration), Observation of an anisotropy in the Galactic cosmic ray arrival direction at 400 TeV with IceCube, Astrophys. J. **746**, 33 (2012).
[15] M. G. Aartsen *et al.* (IceCube Collaboration), Observation of cosmic ray anisotropy with the IceTop air shower array, Astrophys. J. **765**, 55 (2013).
[16] T. Stanev, P. L. Biermann, and T. K. Gaisser, Cosmic rays. 4. The spectrum and chemical composition above 10^4 GeV, Astron. Astrophys. **274**, 902 (1993); K. Kobayakawa, Y. Sato, and T. Samura, Acceleration of particles by oblique shocks and cosmic ray spectra around the knee region, Phys. Rev. D **66**, 083004 (2002); L. G. Sveshnikova, The knee in Galactic cosmic ray spectrum and variety in Supernovae, Astron. Astrophys. **409**, 799 (2003); V. S. Ptuskin and V. N. Zirakashvili, On the spectrum of high-energy cosmic rays produced by supernova remnants in the presence of strong cosmic-ray streaming instability and wave dissipation, Astron. Astrophys. **429**, 755 (2005); A. M. Hillas, Can diffusive shock acceleration in supernova remnants account for high-energy galactic cosmic rays?, J. Phys. G **31**, R95 (2005).
[17] A. D. Erlykin and A. W. Wolfendale, A single source of cosmic rays in the range 10^{15} eV to 10^{16} eV, J. Phys. G **23**, 979 (1997); Cosmic rays and the Monogem supernova remnant, Astropart. Phys. **22**, 47 (2004).
[18] V. L. Ginzburg and S. I. Syrovatskii, *The Origin of Cosmic Rays* (Pergamon Press, Oxford, 1964).
[19] V. S. Ptuskin *et al.*, Diffusion and drift of very high energy cosmic rays in galactic magnetic fields, Astron. Astrophys. **268**, 726 (1993); J. Candia, E. Roulet, and L. N. Epele, Turbulent diffusion and drift in galactic magnetic fields and the explanation of the knee in the cosmic ray spectrum, J. High Energy Phys. 12 (2002) 033; J. Candia, S. Mollerach, and E. Roulet, Cosmic ray spectrum and anisotropies from the knee to the second knee, J. Cosmol. Astropart. Phys. 05 (2003) 003.
[20] G. Giacinti, M. Kachelrieß, and D. V. Semikoz, Explaining the spectra of cosmic ray groups above the knee by escape from the Galaxy, Phys. Rev. D **90**, R041302 (2014).
[21] R. Jansson and G. R. Farrar, A new model of the Galactic magnetic field, Astrophys. J. **757**, 14 (2012); The Galactic magnetic field, Astrophys. J. **761**, L11 (2012).
[22] M. S. Pshirkov, P. G. Tinyakov, P. P. Kronberg, and K. J. Newton-McGee, Deriving global structure of the Galactic magnetic field from Faraday rotation measures of extragalactic sources, Astrophys. J. **738**, 192 (2011).
[23] M. S. Pshirkov, P. G. Tinyakov, and F. R. Urban, Mapping UHECRs deflections through the turbulent galactic magnetic field with the latest RM data, Mon. Not. R. Astron. Soc. **436**, 2326 (2013).
[24] A. Oliva *et al.* (AMS-02 Collaboration) (unpublished).
[25] F. C. Jones, A. Lukasiak, V. Ptuskin, and W. Webber, The Modified Weighted Slab Technique: Models and Results, Astrophys. J. **547**, 264 (2001).
[26] W. R. Webber, A. Soutoul, J. C. Kish, and J. M. Rockstroh, Updated Formula for Calculating Partial Cross Sections for Nuclear Reactions of Nuclei with $Z \leq 28$ and $E > 150$ MeV Nucleon–1 in Hydrogen Targets, Astrophys. J. Suppl. Ser. **144**, 153 (2003).
[27] K. Blum, B. Katz, and E. Waxman, AMS-02 Results Support the Secondary Origin of Cosmic Ray Positrons, Phys. Rev. Lett. **111**, 211101 (2013).
[28] W. R. Webber, F. B. McDonald, and A. Lukasiak, Voyager 2: Measurements in the outer heliosphere of the energy spectra of cosmic-ray nuclei from less than 100-MeV nucleon$^{(-1)}$ to more than 1.0-GeV nucleon$^{(-1)}$, Astrophys. J. **599**, 582 (2003).
[29] D. A. Green, The galactic distribution of SNRs, IAU Symposium/Symp-Int. Astron. Union **296**, 188 (2014).
[30] H. Nakanishi and Y. Sofue, Three-dimensional distribution of the ISM in the Milky Way Galaxy: 1. The HI disk, Publ. Astron. Soc. Jpn. **55**, 191 (2003); Three-dimensional distribution of the ISM in the Milky Way Galaxy: II. The molecular gas disk, Publ. Astron. Soc. Jpn. **58**, 847 (2006); see also the comparison in C. Evoli, D. Grasso, and L. Maccione, Diffuse neutrino and gamma-ray emissions of the Galaxy above the TeV, J. Cosmol. Astropart. Phys. 06 (2007) 003.
[31] M. Kachelrieß and D. V. Semikoz, Reconciling the ultrahigh energy cosmic ray spectrum with Fermi shock acceleration, Phys. Lett. B **634**, 143 (2006).
[32] M. Iacobelli *et al.*, Studying Galactic interstellar turbulence through fluctuations in synchrotron emission: First LOFAR

Galactic foreground detection, Astron. Astrophys. **558**, A72 (2013); see also G. Bernardi, A. G. de Bruyn, G. Harker *et al.*, Foregrounds for observations of the cosmological 21 cm line. II. Westerbork observations of the fields around 3C 196 and the North Celestial Pole, Astron. Astrophys. **522**, A67 (2010); A. Ghosh, J. Prasad, S. Bharadwaj, S. S. Ali, and J. N. Chengalur, Characterizing foreground for redshifted 21 cm radiation: 150 MHz Giant Metrewave Radio Telescope observations, Mon. Not. R. Astron. Soc. **426**, 3295 (2012).

[33] Y. S. Yoon *et al.*, Cosmic-ray proton and helium spectra from the first CREAM flight, Astrophys. J. **728**, 122 (2011).

[34] O. Adriani *et al.* (PAMELA Collaboration), PAMELA Measurements of cosmic-ray proton and helium spectra, Science **332**, 69 (2011).

[35] A. Haungs (private communication).

[36] V. Berezinsky, A. Z. Gazizov, and S. I. Grigorieva, On astrophysical solution to ultrahigh-energy cosmic rays, Phys. Rev. D **74**, 043005 (2006); V. S. Berezinsky, S. I. Grigorieva, and B. I. Hnatyk, Extragalactic UHE proton spectrum and prediction for iron-nuclei flux at 10^8–10^9 **GeV**, Astropart. Phys. **21**, 617 (2004); R. Aloisio, V. Berezinsky, P. Blasi, A. Gazizov, S. Grigorieva, and B. Hnatyk, A dip in the UHECR spectrum and the transition from galactic to extragalactic cosmic rays, Astropart. Phys. **27**, 76 (2007).

[37] C. T. Hill, D. N. Schramm, and T. P. Walker, Implications of the ultrahigh-energy cosmic-ray spectrum observed by the Flys Eye detector, Phys. Rev. D **34**, 1622 (1986); J. P. Rachen, T. Stanev, and P. L. Biermann, Extragalactic ultra-high-energy cosmic rays. 2. Comparison with experimental data, Astron. Astrophys. **273**, 377 (1993); D. Allard, E. Parizot, and A. V. Olinto, On the transition from galactic to extragalactic cosmic-rays: Spectral and composition features from two opposite scenarios, Astropart. Phys. **27**, 61 (2007).

[38] T. Antoni *et al.* (KASCADE Collaboration), KASCADE measurements of energy spectra for elemental groups of cosmic rays: Results and open problems, Astropart. Phys. **24**, 1 (2005).

[39] M. Amenomori *et al.* (TIBET III Collaboration), The all-particle spectrum of primary cosmic rays in the wide energy range from 10^{14} eV to 10^{17} eV observed with the Tibet-III air-shower array, Astrophys. J. **678**, 1165 (2008).

[40] A. Aab *et al.* (Antoine Letessier-Selvon for The Pierre Auger Collaboration), Highlights from the Pierre Auger Observatory, Braz. J. Phys. **44**, 560 (2014).

[41] E. Parizot, Cosmic ray origin: Lessons from ultra-high-energy cosmic rays and the galactic/extragalactic transition, Nucl. Phys. B, Proc. Suppl. **256–257**, 197 (2014).

[42] M. Lemoine, K. Kotera, and J. Pétri, On ultra-high energy cosmic ray acceleration at the termination shock of young pulsar winds, arXiv:1409.0159.

[43] A. Neronov and D. V. Semikoz, Origin of TeV Galactic cosmic rays, Phys. Rev. D **85**, 083008 (2012).

[44] The experimental values $\tilde{d}$ are connected to the actual dipole amplitude d by $\tilde{d} = d_\perp/\langle\cos(\delta)\rangle$, where $d_\perp$ is the dipole component in the equatorial plane and $\langle\cos(\delta)\rangle$ the average declination of the events used in the harmonic analysis based only on R. A.; see e.g. J. Aublin and E. Parizot, Generalized 3D-reconstruction method of a dipole anisotropy in cosmic-ray distributions, Astron. Astrophys. **441**, 407 (2005).

[45] M. Kachelrieß and P. D. Serpico, The Compton-getting effect on ultra-high energy cosmic rays of cosmological origin, Phys. Lett. B **640**, 225 (2006).

[46] V. N. Zirakashvili, Cosmic ray anisotropy problem, Int. J. Mod. Phys. A **20**, 6858 (2005).

[47] P. Mertsch and S. Funk, Solution to the Cosmic Ray Anisotropy Problem, Phys. Rev. Lett. **114**, 021101 (2015).

[48] G. Giacinti, M. Kachelrieß, D. V. Semikoz, and G. Sigl, Cosmic ray anisotropy as signature for the transition from galactic to extragalactic cosmic rays, J. Cosmol. Astropart. Phys. 07 (2012) 031.

[49] G. Giacinti, M. Kachelrieß, and D. V. Semikoz, Filamentary Diffusion of Cosmic Rays on Small Scales, Phys. Rev. Lett. **108**, 261101 (2012).

[50] M. C. Beck *et al.*, A new prescription for the random magnetic field of the Milky Way, arXiv:1409.5120.

[51] G. Giacinti, M. Kachelrieß, D. V. Semikoz, and G. Sigl, Ultrahigh energy nuclei in the turbulent Galactic magnetic field, Astropart. Phys. **35**, 192 (2011).

[52] G. Giacinti, X. Derkx, and D. V. Semikoz, Search for single sources of ultra high energy cosmic rays on the sky, J. Cosmol. Astropart. Phys. 03 (2010) 022.

[53] G. Giacinti, M. Kachelrieß, D. V. Semikoz, and G. Sigl, Ultrahigh energy nuclei in the galactic magnetic field, J. Cosmol. Astropart. Phys. 08 (2010) 036.

[54] J. H. Adams, Jr. *et al.* (EUSO Collaboration), The JEM-EUSO Mission: Status and prospects in 2011, contributions to the 32nd International Cosmic Ray Conference, Beijing, 2011, arXiv:1204.5065.

[55] M. I. Panasyuk *et al.*, The current status of orbital experiments for UHECR studies, arXiv:1501.06368.

[56] M. Kachelrieß and S. Ostapchenko, Neutrino yield from Galactic cosmic rays, Phys. Rev. D **90**, 083002 (2014).

[57] B. C. Lacki and R. Beck, The equipartition magnetic field formula in starburst galaxies: Accounting for pionic secondaries and strong energy losses, Mon. Not. R. Astron. Soc. **430**, 3171 (2013).

[58] R. Aloisio and V. S. Berezinsky, Anti-GZK effect in UHECR diffusive propagation, Astrophys. J. **625**, 249 (2005).

[59] A. Neronov and I. Vovk, Evidence for strong extragalactic magnetic fields from Fermi observations of TeV blazars, Science **328**, 73 (2010); F. Tavecchio *et al.*, The intergalactic magnetic field constrained by Fermi/LAT observations of the TeV blazar 1ES 0229 + 200, Mon. Not. R. Astron. Soc. **406**, L70 (2010); K. Dolag, M. Kachelrieß, S. Ostapchenko, and R. Tomàs, Lower limit on the strength and filling factor of extragalactic magnetic fields, Astrophys. J. **727**, L4 (2011).

[60] P. Blasi, S. Burles, and A. V. Olinto, Cosmological magnetic fields limits in an inhomogeneous universe, Astrophys. J. **514**, L79 (1999); D. Paoletti and F. Finelli, Constraints on a stochastic background of primordial magnetic fields with WMAP and South Pole Telescope data, Phys. Lett. B **726**, 45 (2013).

[61] G. Giacinti, M. Kachelrieß, and D. V. Semikoz, Diffuse cosmic ray, gamma-ray and neutrino fluxes from normal and starburst galaxies (in preparation).

[62] M. G. Aartsen *et al.* (IceCube Collaboration), Observation of High-Energy Astrophysical Neutrinos in Three Years of IceCube Data, Phys. Rev. Lett. **113**, 101101 (2014).

[63] M. G. Aartsen *et al.* (IceCube Collaboration), Atmospheric and astrophysical neutrinos above 1 TeV interacting in IceCube, Phys. Rev. D **91**, 022001 (2015).

[64] A. Neronov, D. V. Semikoz, and C. Tchernin, PeV neutrinos from interactions of cosmic rays with the interstellar medium in the Galaxy, Phys. Rev. D **89**, 103002 (2014).

[65] W. B. Atwood *et al.* (Fermi/LAT Collaboration), The large area telescope on the fermi gamma-ray space telescope mission, Astrophys. J. **697**, 1071 (2009).

[66] A. Neronov and D. Semikoz, Neutrinos from extra-large hadron collider in the Milky Way, arXiv:1412.1690.

[67] V. Savchenko, M. Kachelrieß, and D. V. Semikoz, Imprint of single sources on the cosmic ray anisotropy (in preparation).

[68] K. H. Kampert and M. Unger, Measurements of the cosmic ray composition with air shower experiments, Astropart. Phys. **35**, 660 (2012).